ACS SENSORS

Article

pubs.acs.org/acssensors

Molecular Imprinting of Complex Matrices at Localized Surface Plasmon Resonance Biosensors for Screening of Global Interactions of Polyphenols and Proteins

Joana Rafaela Lara Guerreiro,[†,‡,§] Vladimir E. Bochenkov,[§,∥] Kasper Runager,[§] Hüsnü Aslan,[§] Mingdong Dong,[§] Jan J. Enghild,[§,⊥] Victor De Freitas,[‡] Maria Goreti Ferreira Sales,[†] and Duncan S. Sutherland*[,§]

[†]BioMark Sensor Research-CINTESIS, Instituto Superior de Engenharia do Porto, Porto 4200-072, Portugal

[‡]REQUIMTE/LAQV, Departamento de Química e Bioquímica, Faculdade de Ciências da Universidade do Porto, Porto 4169-007, Portugal

[§]Interdisciplinary Nanoscience Center (iNANO), Aarhus University, Aarhus 8000, Denmark

[∥]Department of Chemistry, Lomonosov Moscow State University, Moscow 119991, Russia

[⊥]Department of Molecular Biology and Genetics, Aarhus University, Aarhus 8000, Denmark

Supporting Information

ABSTRACT: Molecular imprinting polymers (MIP) have been applied to capture and stabilize complex protein matrices at plasmonic sensor surfaces. Ultrathin MIP layers at the surface of gold nanodisks enable the label free quantification of global interactions of polyphenols with protein mixtures. Separate polyphenols (catechin, procyanidin B3- catechin dimer, and PGG-pentagalloyl glucose) give specific and different binding levels to the MIP supported saliva plasmonic sensor. The demonstrated biosensor has application to study bioavailability of polyphenols or evaluation of local retention of small drug molecules.

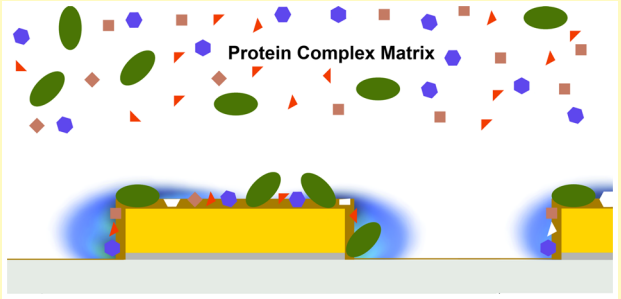

KEYWORDS: *localized surface plasmon resonance (LSPR), molecular imprinting, complex protein matrix, polyphenols, biosensing, nanodisks*

Polyphenols, present in dietary fruit and vegetables, are proposed to aid in prevention of a broad range of diseases such as Alzheimer's,[1−3] Parkinson's,[1] coronary heart diseases,[4−6] and cancer,[7−9] as well as provide antibacterial,[10,11] antiviral,[10] anticarcinogenic,[12−14] and anti-inflammatory[15−17] activities. The specific roles of polyphenols in biological processes are not fully understood but have been highlighted as a group of promising therapeutic or protective agents regarding their ability to bind to proteins or block active sites.[8,18−22] Polyphenols, in common with many small drug molecules, exhibit a broad and varied association with proteins and other biomolecules, which has strong impact on their bioavailability. The first barrier to bioavailability is inside the mouth, where polyphenols interact with salivary proteins, such as amylase (AMY), mucins, and proline-rich proteins (PRP) altering the composition and concentrations available for uptake in the digestive tract. Polyphenols reaching their site of action, either via digestion or therapeutic delivery, will bind to the complex protein environment giving a complex set of global interactions likely determining their effect. Currently, there is a lack of effective tools to study and characterize the specific and global interactions between small molecules, such as polyphenols and complex protein matrices.

Localized surface plasmon resonances (LSPR) have been applied to give high sensitivity label-free optical detection and quantification.[23] Moreover, LSPR approaches have more localized volumes of detection than conventional surface plasmon resonance techniques, allowing higher sensitivity for thin sensor films and less influence of bulk changes in refractive index. Biomolecular recognition elements (typically antibodies[24]) immobilized at the surface of a metal nanostructure act to concentrate the analyte within the local optical field of the plasmonic resonance. Other specific molecular interactions have been applied including DNA−DNA,[25] aptamer−protein,[26,27] protein−protein,[28,29] enzyme−substrate,[30] and protein−small compound.[31,32]

Molecular imprinted polymers (MIP) are an attractive alternative to antibodies[33] due to their inherent stability and short time preparation. The cross-linking of functional

Received: August 20, 2015
Accepted: December 25, 2015
Published: December 25, 2015

DOI: 10.1021/acssensors.5b00054
ACS Sens. 2016, 1, 258−264

monomers around a target molecule enables the formation of specific recognition sites, which allows the targeting of a specific protein by a complex polymer surface. The recognition sites are shaped and sized according to the template/target protein positioning and orientation, resulting from the self-assembling mechanism of functional monomer units. As a result molecular imprinting gives both the ability for each cavity to selectively recognize and stabilize a target molecule from a complex matrix as well as to make sensor surfaces reusable. For LSPR sensors, MIP can provide a thin sensing layer, targeting the high sensitivity/high optical field regions around the nanosensor which has been recently demonstrated.[34] To date, MIP layers have been used to recognize single specific analytes from a mixture.

Here, we report for the first time the molecular imprinting and stabilization of a complex protein matrix. We demonstrate a novel application of molecular imprinting and plasmonics to capture a matrix of human saliva proteins close to the surface of an LSPR sensor. The reusable plasmonic sensor combined molecular imprinting to capture a representative set of a complex protein matrix instead of the traditional application to selective capture a single analyte from a complex matrix.

Here, a natural complex matrix of salivary proteins was immobilized to simulate the oral cavity environment. We applied the complex sensor to follow the interactions of specific polyphenols (pentagalloyl glucose (PGG), procyanidin B3, and (+)-catechin) with human saliva, giving insight into the molecular diversity of polyphenol retention and activity in the oral cavity. The developed concept can be applied to bioavailability studies of polyphenols and other small molecules in a range of protein matrices and give information about tissue specific polyphenol binding affinity and local retention.

EXPERIMENTAL SECTION

Au Nanodisks Fabrication. The Au nanodisks array was prepared based on our previous work.[32]

Molecular Imprinted Films. The imprinting process of both single (amylase) and multiple proteins matrix (saliva) started by creating anchor spots to link the imprinting polymer to the Au nanodisks surface. For that, the Au nanodisk substrates were first incubated overnight in 1 mL of thiophenecarboxylic acid 5 mM prepared in 10% ethanol. The proteins matrix (50 μL of AMY 10 μM or pure saliva) was physically adsorbed by incubating for 2 h at 4 °C followed by MQ water rinsing. The functional monomers (methacrylic acid and (vinylbenzyl)trimethylammonium chloride, 5 mM) were then added for 30 min each followed by overnight (12 h) polymerization by 1 mL of polymerization mixture containing ethylene glycol dimethacrylate, methyl acrylate, and ammonium persulfate 5 mM at 39 °C. After polymerization, the template removal was carried out by adding 50 μL of Proteinase K 500 μg/mL for 2 h at 37 °C. Nonimprinted materials were produced in parallel in the same way, but without the protein step.

LSPR Interaction Studies in a Flow System. Prior to interaction studies with polyphenol (catechin, PGG and B3), the rebinding step was performed by adding 100 μL of pure saliva and AMY to the imprinted surfaces. The polyphenol interacted individually with AMY or saliva, by injecting several standard solutions of increasing concentrations; for PGG, concentrations ranged from 0.1 to 955 μM; for catechin, concentrations ranged from 160 to 56 500 μM, and B3 100−57 000 μM at a flow rate of 50 μL/min. The spectra were collected by measuring the incident light that passes through the flow cell composed by the Au nanodisks substrates. The polyphenol and protein interacted for 2.5 min followed by 2.5 min of rinsing with buffer before spectra collection.

The overall modification steps were performed in steady state conditions, whereas their evaluation was in continuous flow mode.

RESULTS AND DISCUSSION

Molecular Imprinting Procedure on Au Nanodisks. Both saliva and α-amylase (AMY) were surface imprinted at LSPR sensor surfaces. Gold nanodisk LSPR sensors were fabricated on glass substrate by hole mask colloidal lithography.[35] The process (shown in Figure 1) used a 100 nm diameter colloidal template adsorbed on 200 nm polymer films followed by deposition of a 20 nm Titanium film evaporated by physical vapor deposition (PVD) to generate the hole-mask. Subsequently, 2 nm Ti and 20 nm Au were evaporated by PVD followed by mask lift-off to create Au disks. Full details are found in the Supporting Information.

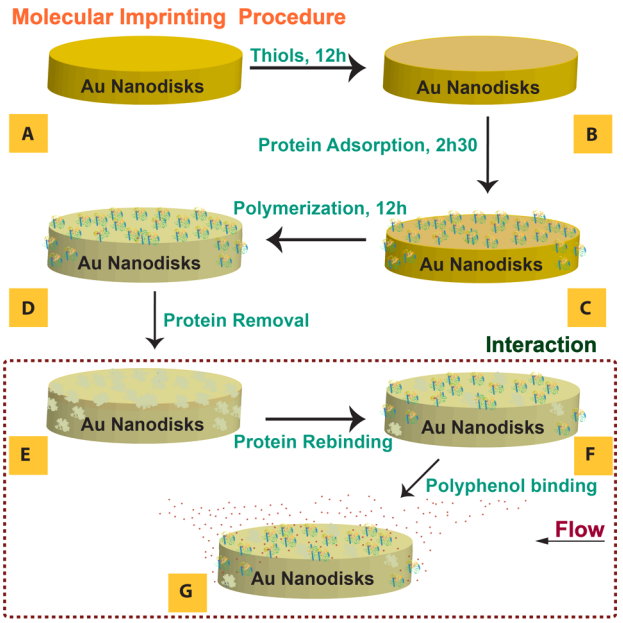

Figure 1. Schematic representation of MIP-Au nanodisks surface imprinting followed by LSPR detection of small molecules. (A) Bare Au nanodisks. (B) Thiophenecarboxylic acid thiol added to Au nanodisks. (C) AMY or saliva adsorption. (D) Free radical polymerization of MIP. (E) Enzymatic protein removal, proteinase K. (F) AMY or saliva incubation. (G) Polyphenol interaction with protein on the surface.

Surface imprinting[36,37] was applied to proteins preadsorbed at the nanodisks surfaces. Briefly, the imprinting process consisted of three main steps. First, a thiol layer was introduced overnight on the Au disks substrates playing an anchoring role between the disks and the imprinting material. The following step involved the physical adsorption of dense AMY or saliva layer (characterized by SDS PAGE, Supporting Information) on Au nanodisks for 2 h. Characterization of the preadsorbed protein layer was carried out by both surface plasmon resonance (SPR) and LSPR measurements combined with the known AMY crystal structure and using a random sequential adsorption model[38] (see Supporting Information Table S-2). The adsorbed AMY formed a thin, dense monolayer, whereas the complex protein layer forming from saliva formed a substantially thicker layer. Protein imprinting is a complex process that can be complicated by proteins' conformational change; therefore, we used water-soluble monomers, cross-linkers, and initiators under mild conditions. Molecular imprinting binding sites formation included both negatively and positively charged monomers. The negative and

DOI: 10.1021/acssensors.5b00054
ACS Sens. 2016, 1, 258−264

positive monomers were added to the surface with adsorbed protein (AMY or Saliva) for 30 min each, and washed with Milli-Q water, followed by an overnight polymerization in the presence of neutral monomer/cross-linker and an initiator solution at 39 °C. The nature and outer surface structure of the proteins determined the localization of several charged groups over its entire surface. Therefore, before polymerization, charged monomers were allowed to establish noncovalent ionic interactions with the numerous protein charged spots (template) of opposite charge. The in situ polymerization process generated a network interlinking the charged monomers and the surface. The formed molecular imprint films were thinner than the expected sizes of the proteins which suggest that only the lower part of the protein was imprinted under the used conditions. In contrast to the binding sites, the surroundings are composed of neutral monomer which reduces nonspecific binding.[39] Finally, the third stage was the template removal, carried out at 39 °C by proteinase K, an efficient enzyme for protein digestion. The imprinting process allowed the production of two distinct smart materials: the AMY imprinted material (AIM) and the saliva imprinted material (SIM) on Au nanodisks. These smart materials were then used for template (AMY or saliva) rebinding followed by polyphenol interaction. As control, a nonimprinted polymer material (NIP) without protein adsorption was also produced on Au nanodisk substrates. The imprinting process details are described and confirmed by an electrochemical technique in the Supporting Information. The imprinting process was followed by characterization of the LSPR, by optical extinction spectroscopy (Shimadzu 3600 UV-vis-NIR).

The fabrication process brings in a small but significant sample to sample variation in the position and amplitude of the resonant optical extinction maxima, giving initial peak positions of 685 ± 11 nm in phosphate buffered saline (PBS), pH 7. This variation in the initial peak position has a negligible effect on the refractive index sensitivity allowing direct comparison of refractive index induced peak shifts. The imprinting process was followed by LSPR detection in a continuous flow system. Extinction spectra were collected while PBS running buffer was flowing through the chamber. The modifications steps measured by LSPR can be seen in Figure 2.

The physical adsorption of AMY and saliva on Au nanodisks induced an average peak shift of 1.94 ± 0.29 and 4.64 ± 1.04 nm, respectively, resulting from the increased refractive index close to the metal surface giving rise to a red shift of the plasmon peak. The formation of the polymer imprinting layers (combined with any associated removal of bound protein) resulted in an overall increased local refractive index of the Au nanodisks. This resulted in an additional red shift of 0.50 ± 0.01 and 1.18 ± 0.32 nm for AIM and SIM, respectively, while the peak shift of the control NIP was 1.60 ± 0.69 nm. Proteinase K was selected as the template removal agent, leading to a blue shift of 1.10 ± 0.31 and 1.81 ± 0.58 nm for AIM and SIM (corresponding to a reduction of refractive index close to the Au nanodisks), respectively, and a red shift of 0.38 ± 0.25 nm for NIP. These results suggest that protein fragments were removed from the binding sites at the MIP surfaces, while for the NIP the small red shift observed may be due to weakly adsorbed proteinase K molecules. All the details regarding the modification process and LSPR measurements are present in Supporting Information Figure S-3. The imprinting process was confirmed by a parallel electrochemical

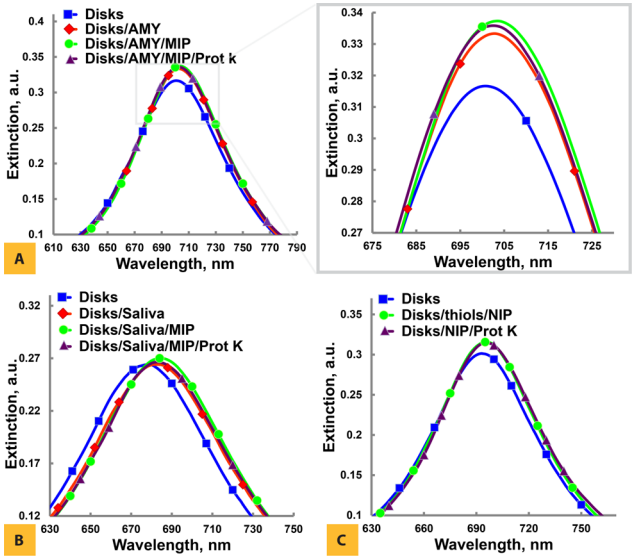

Figure 2. LSPR spectral response for the molecular imprinting process (MIP). (A) AMY imprinting, (B) saliva imprinting, and (C) nonimprinted polymer (NIP). Blue line corresponds to bare Au nanodisks (square), red line to AMY 10 μM or saliva adsorption (inverted square), green line to polymer polymerization (circles), and purple line to protein removal (triangle).

study using flat gold electrodes, as can be seen in Figures S-4 and 5 and Tables S-3 and 4 in the Supporting Information.

The decay length of the field enhancement around the Au nanodisks surface was previously estimated by FDTD simulations to be 17.7 ± 0.7 nm.[32,40] It is known that the sensitivity decreases dramatically with the increasing distance from the surface. The polymer thickness with imprinted saliva was evaluated by atomic force microscopy (AFM) imaging showing a thin molecular imprinted polymer thickness of ∼4 nm on top of the Au nanodisks and ∼0.5 nm on the glass substrate between the disks (Figure S-6 in the Supporting Information). The imprinted and nonimprinted AMY polymer substrates were also measured by AFM in liquid shown in Figure 3, and details are found in the Supporting Information.

The presence of the template AMY led to a clearly altered topography at the sensor surface compared to the nonimprinted surface indicating that the imprinting process occurred at the nanodisk surface.

Rebinding Capability. Protein entrapment can be an issue for protein rebinding due to possible steric hindrance limitations; thus it is essential to promote a good protein removal. The use of thin polymers might be advantageous to facilitate protein removal. Both smart surfaces AIM and SIM were tested to evaluate rebinding capability. The results obtained for AMY rebinding on AIM and saliva rebinding on SIM (2 h) provided an LSPR red shift of 0.99 ± 0.35 and 1.79 ± 0.28 nm, respectively, correlating very well with the blue shift promoted by template removal, indicating a good rebinding capability. The protein removal from the multiple used smart materials provided an LSPR blue shift consistent with the previous results, 0.94 ± 0.40 nm for AMY and 1.71 ± 0.58 nm for saliva, showing the reusability of MIP samples (Table S-5 in the Supporting Information). Both saliva and AMY were also incubated on the NIP surface, promoting an additional peak shift of 1.21 ± 0.28 and 0.57 ± 0.21 nm, respectively. These results indicate that as expected both AMY and saliva can bind nonspecifically to surfaces with the AMY binding being

DOI: 10.1021/acssensors.5b00054
ACS Sens. 2016, 1, 258−264

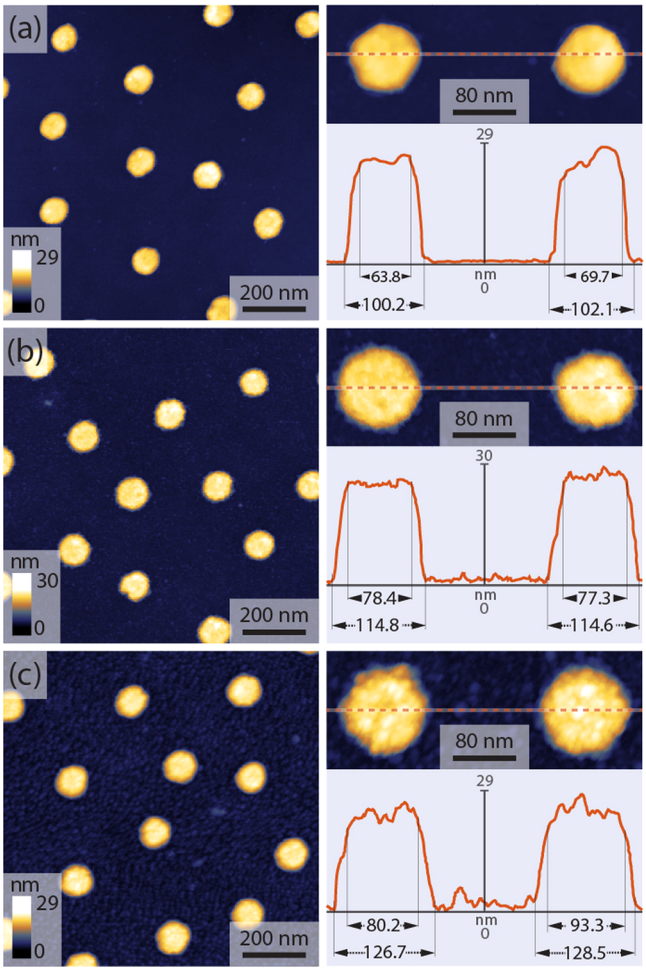

Figure 3. AFM images in liquid of (a) Au nanodisks (control), (b) nonimprinted material, and (c) amylase imprinted on Au nanodisks substrate.

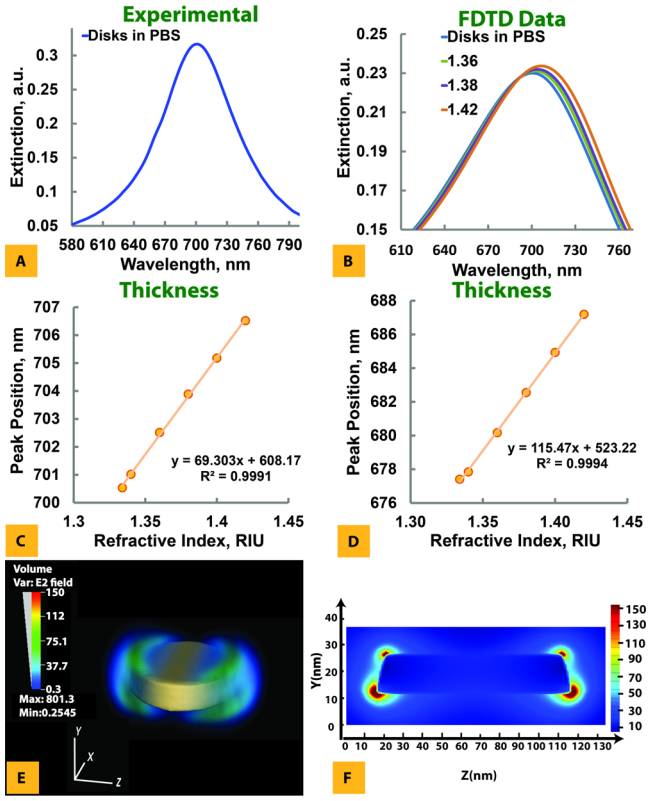

Figure 4. Experimental (A) and FDTD simulated (B) extinction spectra of Au nanodisks substrates immersed in different refractive index solutions. Correlation peak position vs refractive index units through FDTD for 7 nm (C) and 14 nm (D) layer thickness. (E) Field enhancement (E^2 scale 0−150) distribution image of the Au nanodisks. (F) Two-dimensional cross section field map.

comparable to that of the AMY MIP. The saliva imprinted surface provides more robust and higher specific responses. The capture of target proteins from saliva as achieved through the molecular imprinting of Au disks, with the salivary proteins being immobilized and available for use as a sensor element.

FDTD Calculations. Finite-difference time-domain (FDTD) calculations of the Au nanodisks optical response were performed by matching to the experimental extinction spectra and determined sensitivities, plotted in Figure 4. Experimental and FDTD spectra present similar peak shapes and positions although relative intensity is slightly different. Additionally, both spectra with peaks resulting from a dipole resonance are in good agreement, Figure 4A and B. FDTD simulations matched, as a starting point, the Au nanodisks dimensions of 100 nm diameter by 22 nm height (20 nm Au with 2 nm Ti adhesion layer) and the corresponding experimental extinction peak. The Au nanodisk modification led to an LSPR peak shift which is directly correlated with experimental bulk refractive index changes. The sensitivity to refractive index changes in thin films was measured by variation of the films refractive index in the FDTD model and assuming a maximum thickness of 7/14 nm for the AMY and saliva films, respectively. The obtained calibration curves for 7 and 14 nm films are plotted in Figure 4C and D. Measurements by SPR on homogeneous surfaces indicated a surface coverage of AMY consistent with a side on configuration of AMY with maximum footprint (AMY size is indicated to be 11.5 × 11.9 × 7.0 nm^3) which points to an AMY thickness of 7 nm. Salivary proteins are known to form thicker layers,[41] and here we assumed that the layer thickness was 14 nm, roughly determined based on the protein composition of saliva and their three-dimensional size. The final refractive index of the saliva layer using calibration from FDTD simulations, assuming a 14 nm layer thickness, was 1.38 which fits well with the refractive indices measured on adsorbed saliva films.[41]

FDTD also provided additional information about the spatial confinement of the plasmon induced near−field, which indicates that highest values of the near-field enhancement of the incoming optical field are localized around the upper and lower rims of the Au nanodisk, as can be seen in Figure 4E. The outcome of FDTD calculations allows the quantification of the rebinding of protein and the amount of interacting polyphenols.

Binding Affinities. In this work, we carry out proof of principle studies of the interaction of different polyphenol compounds with the complex saliva MIP. Polyphenols from different classes, flavonoid and nonflavonoid, were tested. Three polyphenols were selected for the binding affinity studies: PGG from the nonflavonoid class consisting of a glucose molecule esterified with five gallic acid and two different structural catechins; (+)-catechin and procyanidin dimer B3 [(+)-catechin-(4−8)-(+)-catechin].

DOI: 10.1021/acssensors.5b00054
ACS Sens. 2016, 1, 258−264

Each polyphenol was injected in the flow system interacting with the protein content on both AIM and SIM surfaces, while control NIP and AIM/SIM without protein rebinding were also evaluated. Generally, the imprinted materials provided better response than nonimprinted materials, Figure S-7, Supporting Information. Additionally, the obtained signals when using saliva are significantly higher than those for the tests with AMY. The imprinted material with no rebinding was used as a control providing the lower signal (Table S-6 and Figure S-7 in the Supporting Information). Binding characteristics were measured by repeated injection of increasing concentrations of PGG ranging 0.1−955 μM, catechin 160−56 500 μM, and B3 100−57 000 μM, all shown in Figure 5.

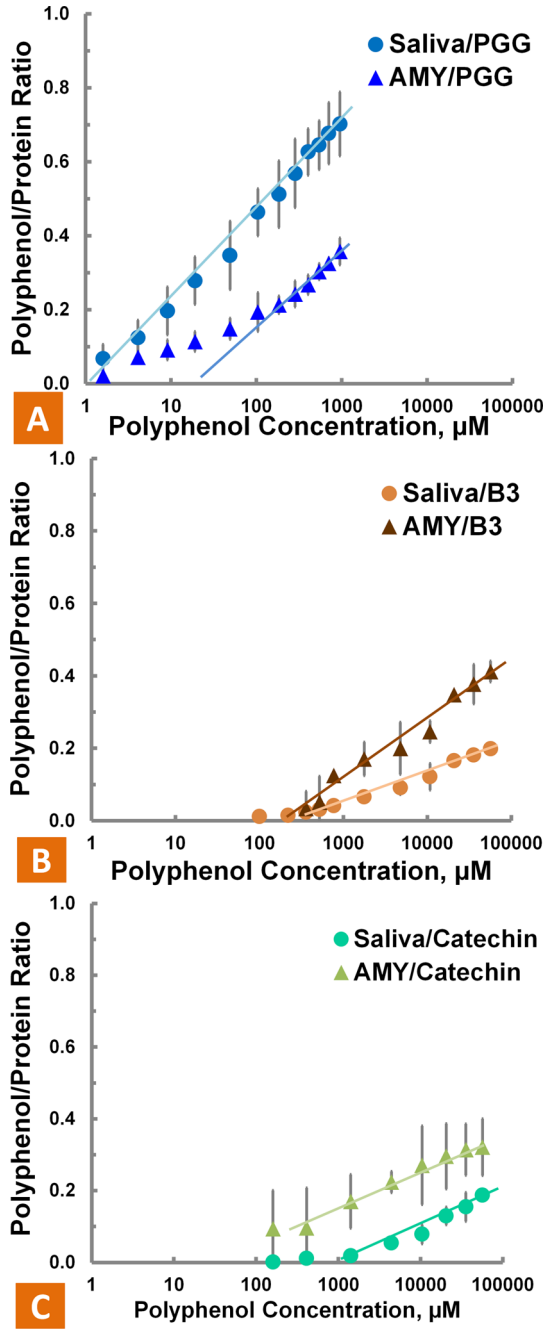

Figure 5. Ratio of polyphenols mass/protein mass for (A) PGG, (B) B3, and (C) catechin. AMY (triangles) and saliva (circles).

When PGG, catechin or B3 were injected in the system, they interacted with surface bound protein and gave red shifts of the plasmon peak that remained after rinsing indicating a strong interaction. The obtained shifts indicate a linear dependence with log Polyphenol concentration (LSPR λ_{max} shift vs log concentration). Though, for all polyphenols, the linear response was only achieved for a smaller region within the tested concentration range.

The signal from PGG binding to the LSPR sensor surface (Figure S-7, Supporting Information) showed a consistently higher binding at MIP surfaces compared to NIP. The difference was much larger for saliva surfaces compared to AMY surfaces, which correlated to an overall lower protein binding of the AMY. The variation in the measurements for the NIP surfaces was substantially larger than MIP surfaces that may result from weaker or more variable protein-NIP surface interactions. Binding of polyphenols directly to the polymer surface in the absence of protein, showed a low but significant level. When protein is attached to the surface (in particular for the saliva surfaces) it likely reduces this background binding both competing for PGG adsorption and blocking the surface. We correlate the PGG binding to the amount of protein in order to estimate the binding characteristics. The quantification for the AMY assumed a 7 nm layer while that of the saliva used a 14 nm layer. It should be noted that the ratio of the amount of polyphenol to protein is unaffected by the assumed thickness. In Figure 5A, the ratio of polyphenol mass/protein mass is plotted versus polyphenol concentration (log scale). This mass ratio can be indirectly corrected with the peak shift through the refractive index increment which is higher by a factor of 3 for PGG (0.532 cm^2/g experimentally measured value) in comparison with the protein (0.180 cm^2/g literature value[42]). PGG binding to saliva is higher than binding to AMY (~2 times higher). We cannot rule out a contribution of PGG binding directly to the MIP surface; however, the PGG binding to AMY corresponds to around 20−25 PGGs/protein for the highest concentration which is comparable to that previously observed for PGG binding to AMY covalently attached to surfaces.[32] The stronger PGG attachment to the complex protein mixture of saliva (we observe more than 36 proteins at the MIP layer by mass spectrometry including AMY; see Table S-7 in the Supporting Information) indicates that other proteins within the saliva are significantly stronger binders for PGG than AMY, suggesting that sensors based on specific single proteins (even those which are the most abundant) risk wrongly evaluating the global response. The binding profiles for PGG showed a linear regime (in the log scale) at higher concentrations but with significant deviations toward higher binding at low concentrations suggesting that there are ranges of binding strength sites at the proteins (which has been observed before for PGG binding to AMY). The overall amount of PGG molecules binding reaches a very high level at higher concentrations at the saliva. While we cannot calculate the number of PGG molecules binding to each protein in saliva we estimate the binding to an AMY sized protein would on average be ~40 which indicates that protein unfolding reveals additional binding sites or that PGG cluster growth occurs at already bound PGG molecules.

We applied our sensing approach to study the differences between polyphenol interaction with proteins. The combination of ultrathin MIP layer with LSPR allowed us to evaluate the binding of two small polyphenols (the monomeric basic unit of condensed tannins, (+)-catechin MW 290.3, and a

DOI: 10.1021/acssensors.5b00054
ACS Sens. 2016, 1, 258−264

catechin dimer, the procyanin-B3 MW 2 × 290.3) and the PGG (MW 940.7), with both AMY and saliva.

The LSPR signals for B3 (Figure S-7B, Supporting Information) and catechin (Figure S-7C, Supporting Information) were significantly lower compared to that for the PGG as might be expected from their lower molecular weight; however, significantly larger concentrations of the polyphenols were required to induce binding, indicating a concomitant weaker interaction (see Figure 5). Binding to the polymer surface in the absence of the protein was also significantly lower than for PGG. Interestingly, the two smaller polyphenols studied showed different profiles of binding to AMY versus saliva. B3 binding to AMY was stronger (~factor of 2) than to the complex saliva protein mixture and higher binding tendency with the increase of B3 concentration. While for catechin the binding to AMY is higher than to the saliva complex but with similar binding tendency with increased catechin concentration, also suggesting a stronger interaction. This fact could indicate that AMY has a limited number of higher binding sites while the complex of saliva proteins has some proteins with substantial numbers of low binding strength sites. The signal levels observed for the catechin binding with its low molecular weight to AMY were similar to those for the maximal binding observed at nonprotein covered surface (albeit at higher concentrations of catechin) and with significant errors indicating that the catechin binding to AMY is likely close to the detection limit for our system.

Overall, we observed a significant variation in the binding strength of polyphenols to the complex mixture of saliva proteins compared to binding to one specific protein (AMY). Amylase is shown to bind PGG weakly relative to saliva but to bind B3 and catechin stronger. This demonstrates that for studying global effects of different small molecule binding on proteins, a complex saliva protein mixture has the potential to give a better response than sensors based on single or a few proteins. For polyphenol binding to the complex saliva mixture, we observe a strong variation in binding of specific polyphenols. The effect of a complex food matrix on the protein and polyphenol interaction was also tested showing some interference, although the signal was affected in a very systematic way indicating that for the analysis of complex food matrices a careful choice of an appropriated matrix for calibration needs to be made (Figure S-8, Supporting Information). In the field of food science, this provides a method and proof of principle to study quantitatively both the importance of different polyphenols in astringency but also to understand and correct for the astringency response from specific wines and base ingredients during production. In particular, these approaches may be used to study the bioavailability of polyphenols from food and beverages after passing through the oral environment. A similar concept for studying global binding response of drug molecules to the complex protein environment of tumors or intracellular environment could be applied to estimate retention or local bioavailability of drug molecules in therapeutic situations on the site of action.

The presented results indicate that all three polyphenols showed large affinity with proteins and may interact with multiple binding sites. The binding affinity provides information about barriers to polyphenol transport through interaction with complex protein matrices before its absorption by the organism and consequently about their bioavailability. According to these results it seems that PGG will be the less available polyphenol after passing through the mouth while catechin will be the most available. Catechin is a monomer with low molecular size which may favor its absorption by the intestine lumen.

CONCLUSIONS

Here we have developed a plasmonic biosensor to study global interactions between small molecules and complex protein matrices. We have made use of smart MIP layers which are ultrathin, combining with the high localization of the optical fields around the plasmonic sensor and imprint complex protein matrices to allow the capture and study of saliva and its interaction with polyphenols. The sensor would allow the study of bioavailability of small molecules in food or drug delivery applications associated with a broad range of disorders including neurodegenerative diseases, cardiovascular disease, and cancer.

ASSOCIATED CONTENT

Supporting Information

The Supporting Information is available free of charge on the ACS Publications website at DOI: 10.1021/acssensors.5b00054.

Materials and methods including saliva characterization, Au nanodisks fabrication, molecular imprinted synthesis, and evaluation, interaction measurements by LSPR, electrochemical measurements, as well as description of data analysis; bare Au disks MIP and nonimprinted layer characterized by atomic force microscopy; mass spectroscopy of both pure saliva and Au disks/MIP saliva/rebinding saliva (PDF)

AUTHOR INFORMATION

Corresponding Author

*E-mail: duncan@inano.au.dk.

Author Contributions

The manuscript was written through contributions of all authors. All authors have given approval to the final version of the manuscript.

Notes

The authors declare no competing financial interest.

ACKNOWLEDGMENTS

The authors acknowledge FCT, Fundação para a Ciência e Tecnologia, for the financial support (SFRH/BD/72479/2010), the FSE, Fundo Social Europeu for the cofinancial support. Vladimir Bochenkov acknowledges the support from RFBR Grant #15-03-99582.

REFERENCES

(1) Ehrnhoefer, D. E.; Bieschke, J.; Boeddrich, A.; Herbst, M.; Masino, L.; Lurz, R.; Engemann, S.; Pastore, A.; Wanker, E. E. EGCG redirects amyloidogenic polypeptides into unstructured, off-pathway oligomers. *Nat. Struct. Mol. Biol.* **2008**, *15*, 558−566.

(2) Ono, K.; Yoshiike, Y.; Takashima, A.; Hasegawa, K.; Naiki, H.; Yamada, M. Potent anti-amyloidogenic and fibril-destabilizing effects of polyphenols in vitro: implications for the prevention and therapeutics of Alzheimer's disease. *J. Neurochem.* **2003**, *87*, 172−181.

(3) Porat, Y.; Abramowitz, A.; Gazit, E. Inhibition of amyloid fibril formation by polyphenols: Structural similarity and aromatic interactions as a common inhibition mechanism. *Chem. Biol. Drug Des.* **2006**, *67*, 27−37.

DOI: 10.1021/acssensors.5b00054
ACS Sens. 2016, 1, 258−264

(4) Corder, R.; Mullen, W.; Khan, N. Q.; Marks, S. C.; Wood, E. G.; Carrier, M. J.; Crozier, A. Red wine procyanidins and vascular health. *Nature* **2006**, *444*, 566−566.
(5) Corder, R.; Douthwaite, J. A.; Lees, D. M.; Khan, N. Q.; Viseu dos Santos, A. C.; Wood, E. G.; Carrier, M. J. Endothelin-1 synthesis reduced by red wine - Red wines confer extra benefit when it comes to preventing coronary heart disease. *Nature* **2001**, *414*, 863−864.
(6) Fito, M.; Cladellas, M.; de la Torre, R.; Marti, J.; Munoz, D.; Schroder, H.; Alcantara, M.; Pujadas-Bastardes, M.; Marrugat, J.; Lopez-Sabater, M. C.; Bruguera, J.; Covas, M. I. Anti-inflammatory effect of virgin olive oil in stable coronary disease patients: a randomized, crossover, controlled trial. *Eur. J. Clin. Nutr.* **2008**, *62*, 570−574.
(7) Gescher, A.; Pastorino, U.; Plummer, S. M.; Manson, M. M. Suppression of tumour development by substances derived from the diet - mechanisms and clinical implications. *Br. J. Clin. Pharmacol.* **1998**, *45*, 1−12.
(8) Middleton, E.; Kandaswami, C.; Theoharides, T. C. The effects of plant flavonoids on mammalian cells: Implications for inflammation, heart disease, and cancer. *Pharmacol. Rev.* **2000**, *52*, 673−751.
(9) Aggarwal, B. B.; Shishodia, S. Molecular targets of dietary agents for prevention and therapy of cancer. *Biochem. Pharmacol.* **2006**, *71*, 1397−1421.
(10) Daglia, M. Polyphenols as antimicrobial agents. *Curr. Opin. Biotechnol.* **2012**, *23*, 174−181.
(11) Ferrazzano, G. F.; Amato, I.; Ingenito, A.; Zarrelli, A.; Pinto, G.; Pollio, A. Plant Polyphenols and Their Anti-Cariogenic Properties: A Review. *Molecules* **2011**, *16*, 1486−1507.
(12) Link, A.; Balaguer, F.; Goel, A. Cancer chemoprevention by dietary polyphenols: Promising role for epigenetics. *Biochem. Pharmacol.* **2010**, *80*, 1771−1792.
(13) Izzotti, A.; Cartiglia, C.; Steele, V. E.; De Flora, S. MicroRNAs as targets for dietary and pharmacological inhibitors of mutagenesis and carcinogenesis. *Mutat. Res., Rev. Mutat. Res.* **2012**, *751*, 287−303.
(14) Li, Y. Y.; Zhang, T. Targeting cancer stem cells by curcumin and clinical applications. *Cancer Lett.* **2014**, *346*, 197−205.
(15) Santangelo, C.; Vari, R.; Scazzocchio, B.; Di Benedetto, R.; Filesi, C.; Masella, R. Polyphenols, intracellular signalling and inflammation. *Ann. Ist. Super. Sanita* **2007**, *43*, 394−405.
(16) Albini, A.; Tosetti, F.; Li, V. W.; Noonan, D. M.; Li, W. W. Cancer prevention by targeting angiogenesis. *Nat. Rev. Clin. Oncol.* **2012**, *9*, 498−509.
(17) Potapovich, A. I.; Lulli, D.; Fidanza, P.; Kostyuk, V. A.; De Luca, C.; Pastore, S.; Korkina, L. G. Plant polyphenols differentially modulate inflammatory responses of human keratinocytes by interfering with activation of transcription factors NF kappa B and AhR and EGFR-ERK pathway. *Toxicol. Appl. Pharmacol.* **2011**, *255*, 138−149.
(18) Sinclair, D. A.; Guarente, L. Small-Molecule Allosteric Activators of Sirtuins. In *Annual Review of Pharmacology and Toxicology, Vol 54*; Insel, P. A., Ed.; Annual Reviews: Palo Alto, CA, 2014; Vol. *54*, pp 363−380.
(19) Surh, Y. J. Cancer chemoprevention with dietary phytochemicals. *Nat. Rev. Cancer* **2003**, *3*, 768−780.
(20) Ramos, S. Cancer chemoprevention and chemotherapy: Dietary polyphenols and signalling pathways. *Mol. Nutr. Food Res.* **2008**, *52*, 507−526.
(21) Seeram, N. P.; Zhang, Y. J.; Nair, M. G. Inhibition of proliferation of human cancer cells and cyclooxygenase enzymes by anthocyanidins and catechins. *Nutr. Cancer* **2003**, *46*, 101−106.
(22) Xagorari, A.; Roussos, C.; Papapetropoulos, A. Inhibition of LPS-stimulated pathways in macrophages by the flavonoid luteolin. *Br. J. Pharmacol.* **2002**, *136*, 1058−1064.
(23) Im, H.; Bantz, K. C.; Lee, S. H.; Johnson, T. W.; Haynes, C. L.; Oh, S.-H. Self-Assembled Plasmonic Nanoring Cavity Arrays for SERS and LSPR Biosensing. *Adv. Mater.* **2013**, *25*, 2678−2685.
(24) Truong, P. L.; Kim, B. W.; Sim, S. J. Rational aspect ratio and suitable antibody coverage of gold nanorod for ultra-sensitive detection of a cancer biomarker. *Lab Chip* **2012**, *12*, 1102−1109.
(25) Alivisatos, A. P.; Johnsson, K. P.; Peng, X. G.; Wilson, T. E.; Loweth, C. J.; Bruchez, M. P.; Schultz, P. G. Organization of 'nanocrystal molecules' using DNA. *Nature* **1996**, *382*, 609−611.
(26) Wu, B.; Chen, L. C.; Huang, Y. J.; Zhang, Y. M.; Kang, Y. J.; Kim, D. H. Multiplexed Biomolecular Detection Based on Single Nanoparticles Immobilized on Pneumatically Controlled Microfluidic Chip. *Plasmonics* **2014**, *9*, 801−807.
(27) Balamurugan, S.; Mayer, K. M.; Lee, S.; Soper, S. A.; Hafner, J. H.; Spivak, D. A. Nanostructure shape effects on response of plasmonic aptamer sensors. *J. Mol. Recognit.* **2013**, *26*, 402−407.
(28) Bhagawati, M.; You, C. J.; Piehler, J. Quantitative Real-Time Imaging of Protein-Protein Interactions by LSPR Detection with Micropatterned Gold Nanoparticles. *Anal. Chem.* **2013**, *85*, 9564−9571.
(29) Cohavi, O.; Reichmann, D.; Abramovich, R.; Tesler, A. B.; Bellapadrona, G.; Kokh, D. B.; Wade, R. C.; Vaskevich, A.; Rubinstein, I.; Schreiber, G. A Quantitative, Real-Time Assessment of Binding of Peptides and Proteins to Gold Surfaces. *Chem. - Eur. J.* **2011**, *17*, 1327−1336.
(30) Chen, S.; Svedendahl, M.; Van Duyne, R. P.; Kall, M. Plasmon-Enhanced Colorimetric ELISA with Single Molecule Sensitivity. *Nano Lett.* **2011**, *11*, 1826−1830.
(31) Zhang, J.; Wang, L.; Pan, D.; Song, S.; Boey, F. Y. C.; Zhang, H.; Fan, C. Visual cocaine detection with gold nanoparticles and rationally engineered aptamer structures. *Small* **2008**, *4*, 1196−1200.
(32) Guerreiro, J. R. L.; Frederiksen, M.; Bochenkov, V. E.; De Freitas, V.; Ferreira Sales, M. G.; Sutherland, D. S. Multifunctional Biosensor Based on Localized Surface Plasmon Resonance for Monitoring Small Molecule-Protein Interaction. *ACS Nano* **2014**, *8*, 7958−7967.
(33) Chianella, I.; Guerreiro, A.; Moczko, E.; Caygill, J. S.; Piletska, E. V.; De Vargas Sansalvador, I. M.; Whitcombe, M. J.; Piletsky, S. A. Direct Replacement of Antibodies with Molecularly Imprinted Polymer Nanoparticles in ELISA-Development of a Novel Assay for Vancomycin. *Anal. Chem.* **2013**, *85*, 8462−8468.
(34) Abbas, A.; Tian, L. M.; Morrissey, J. J.; Kharasch, E. D.; Singamaneni, S. Hot Spot-Localized Artificial Antibodies for Label-Free Plasmonic Biosensing. *Adv. Funct. Mater.* **2013**, *23*, 1789−1797.
(35) Fredriksson, H.; Alaverdyan, Y.; Dmitriev, A.; Langhammer, C.; Sutherland, D. S.; Zaech, M.; Kasemo, B. Hole-mask colloidal lithography. *Adv. Mater.* **2007**, *19*, 4297−4302.
(36) Whitcombe, M. J.; Chianella, I.; Larcombe, L.; Piletsky, S. A.; Noble, J.; Porter, R.; Horgan, A. The rational development of molecularly imprinted polymer-based sensors for protein detection. *Chem. Soc. Rev.* **2011**, *40*, 1547−1571.
(37) Li, S.; Cao, S.; Whitcombe, M. J.; Piletsky, S. A. Size matters: Challenges in imprinting macromolecules. *Prog. Polym. Sci.* **2014**, *39*, 145−163.
(38) Hinrichsen, E. L.; Feder, J.; Jossang, T. Geometry of random sequential adsorption. *J. Stat. Phys.* **1986**, *44*, 793−827.
(39) Moreira, F. T. C.; Sharma, S.; Dutra, R. A. F.; Noronha, J. P. C.; Cass, A. E. G.; Sales, M. G. F. Smart plastic antibody material (SPAM) tailored on disposable screen printed electrodes for protein recognition: Application to myoglobin detection. *Biosens. Bioelectron.* **2013**, *45*, 237−244.
(40) Mazzotta, F.; Johnson, T. W.; Dahlin, A. B.; Shaver, J.; Oh, S.-H.; Höök, F. Influence of the evanescent field decay length on the sensitivity of plasmonic nanodisks and nanoholes. *ACS Photonics* **2015**, *2*, 256−262.
(41) Cardenas, M.; Arnebrant, T.; Rennie, A.; Fragneto, G.; Thomas, R. K.; Lindh, L. Human saliva forms a complex film structure on alumina surfaces. *Biomacromolecules* **2007**, *8*, 65−69.
(42) Hook, F.; Voros, J.; Rodahl, M.; Kurrat, R.; Boni, P.; Ramsden, J. J.; Textor, M.; Spencer, N. D.; Tengvall, P.; Gold, J.; Kasemo, B. A comparative study of protein adsorption on titanium oxide surfaces using in situ ellipsometry, optical waveguide lightmode spectroscopy, and quartz crystal microbalance/dissipation. *Colloids Surf., B* **2002**, *24*, 155−170.

DOI: 10.1021/acssensors.5b00054
ACS Sens. 2016, 1, 258−264